Reduced-Order, Radiobiologically Informed Simulation Framework for Magnetic Hyperthermia-Radiation Therapy Scenario Analysis

Dan Heo[1], Farshad Mostafaei[1], John Barrett[1], Chulhaeng Huh[1*]

1. Georgia Cancer Center, Department of Radiation Oncology, Medical College of Georgia, Augusta University, Augusta, Georgia, USA
*Presenting Author

2026 JULY 19–22 VANCOUVER, BC
JOINT AAPM | COMP MEETING

INTRODUCTION

Hyperthermia has long been recognized as a potent sensitizer of radiation therapy (RT), capable of enhancing tumor cell kill through multiple complementary mechanisms, including inhibition of DNA repair, modulation of tumor microenvironment, and overcoming radiation resistance in hypoxic regions. Among emerging hyperthermia modalities, magnetic hyperthermia (MHT) employs iron oxide nanoparticles under an alternating magnetic field to generate localized, controllable heat within the tumor. Although direct intratumoral injection is required for nanoparticle delivery, this approach enables spatially confined heating that preferentially targets the tumor volume while minimizing damage to surrounding normal tissue.

Despite strong preclinical evidence supporting magnetic hyperthermia-radiation therapy (MHRT) as a combined modality, its clinical translation remains limited by the absence of a standardized quantitative framework for treatment evaluation and prescription. Clinically established radiobiological metrics such as equivalent radiation dose in 2 Gy fractions (EQD2) are not directly applicable to combined thermal-radiation treatments, making systematic comparison and optimization difficult.

Our group has been investigating quantitative evaluation of MHRT, including development of EQD-compatible biological models. Building on this foundation, the present study introduces a voxel-based, fractionation-aware radiobiological simulation framework that integrates thermal and radiation effects to compute tumor control probability (TCP) as a function of fraction number, enabling direct comparison of RT, conventional hyperthermia-RT (HTRT), and MHRT.

METHODS AND MATERIALS

Overview: A voxel-based, fractionation-aware radiobiological simulation framework was implemented to integrate radiation dose-response, thermal damage, hypoxia modulation, and radiosensitization within a unified computational environment. Simulations were performed using representative prostate cancer cell line parameters (PC3) under identical RT conditions across three modalities: RT-only, HTRT, and MHRT. All computations were implemented in Python using NumPy.

Tumor Phantom and Geometry: A 10 x 10 x 10 mm cubic tumor phantom was discretized into a 40 x 40 x 40 voxel grid (voxel size: 0.25 mm). Nanoparticle (NP) injection regions were modeled as regularly spaced cylindrical volumes arranged on a hexagonal lattice, reflecting localized intratumoral delivery. Cancer stem cell (CSC) niches were assigned to randomly distributed spherical subregions within the tumor volume.

Per-Fraction Survival Model

(1) Radiation Survival – Linear-Quadratic model: Per-fraction cell survival under RT was computed using the linear-quadratic (LQ) model:

$$SF_{RT} = exp[-\alpha d - \beta d^2] \quad (1)$$

where d (Gy) is the dose per fraction at each voxel, and α (Gy^{-1}) and β (Gy^{-2}) are voxel-wise radiosensitivity parameters. Dose distributions were calculated analytically with exponential attenuation along the beam axis (x-direction from x = 0).

(2) Thermal Damage – Arrhenius / Eyring Model: Thermal cell kill was modeled using the Eyring-Arrhenius formalism. The thermal inactivation rate $k(T)$ at absolute temperature T_k is:

$$k(T_k) = \frac{k_B T_k}{h} exp\left[\frac{\Delta S}{R} - \frac{\Delta H}{RT_k}\right] \quad (2)$$

where k_B is Boltzmann's constant, h is Planck's constant, R is the gas constant (1.987 cal mol^{-1} K^{-1}), and ΔS, ΔH are the entropy and enthalpy of inactivation (cal mol-1), respectively. The cumulative thermal damage Ω and heat-only survival fraction are:

$$\Omega = N_{HT} \cdot k(T) \cdot t_{HT}, \qquad SF_{HT} = exp[-\Omega] \quad (3)$$

where N_{HT} is the number of HT fractions and t_{HT} is the heating duration per session (seconds).

(3) Combined survival: The total per-fraction survival fraction at each voxel is the product of radiation and thermal contributions:

$$SF_{total} = SF_{RT} \times SF_{HT} \quad (4)$$

Radiosensitivity Parameter Modulation: Temperature-dependent radiosensitivity was implemented via log-linear interpolation of α and β between 37 °C and 41 °C values:

$$w_T = \frac{\min(T, 43) - 37}{41 - 37}, \; \alpha(T) = \alpha_{37}\left(\frac{\alpha_{41}}{\alpha_{37}}\right)^{w_T}, \; \beta(T) = \beta_{37}\left(\frac{\beta_{41}}{\beta_{37}}\right)^{w_T} \quad (5)$$

Hypoxia modulation was applied by computing an effective oxygen enhancement ratio (OER) from the voxel-wise hypoxia severity map, which then scaled α and β with independent exponents p and q, respectively (p = *1.0, q = 1.6*). This reflects the greater sensitivity of the quadratic damage component to hypoxia. Radiosensitization from thermal stress was incorporated via an RSI-based enhancement factor η, derived from the Arrhenius damage integral Ω, which further attenuated the OER correction in heated voxels.

For MHRT, NP regions received an additional dose-enhancement factor r_{NP} applied to the per-voxel dose, representing the localized heating and dose-amplification effect of iron oxide nanoparticles.

CSC voxels were assigned reduced α and β values (penalty factors $k_{CSC,\alpha}$ and $k_{CSC,\beta}$) to reflect their higher radioresistance.

Tumor Control Probability (TCP): TCP as a function of fraction number n was estimated using the Poisson clonogen model:

$$TCP(n) = exp[-\sum_i N_{0,i} \cdot S_{cum,i}(n)] \quad (6)$$

where $N_{0,i}$ is the initial clonogen count assigned to voxel i, weighted by CSC density (5x relative to non-CSC voxels), and $S_{cum,i}(n)$ is the cumulative survival at that voxel after n fractions. S_{cum} was defined as the net surviving fraction accumulated over the entire treatment course. For this study, RT was delivered in 40 fractions, with hyperthermia applied every 5th RT fraction.

Equivalent Dose in 2 Gy Fractions (EQD2): To provide a clinically interpretable dose metric, the total biological effect was expressed as EQD2 by inverting the cumulative log-kill under reference conditions (α_{ref}, β_{ref} at 37°C, normoxia; d_{ref} = 2 Gy):

$$D_{eq} = \frac{-lnSF_{total}}{\alpha_{ref} + \beta_{ref} \cdot d_{ref}}, \qquad EQD2 = D_{eq} \cdot \frac{d_{ref}(\alpha_{ref} + \beta_{ref} \cdot d_{ref})}{\alpha_{ref} + 2\beta_{ref}} \quad (7)$$

EQD2 maps were computed for each modality using the RT-baseline radiobiological parameters to enable direct cross-modality comparison.

RESULTS

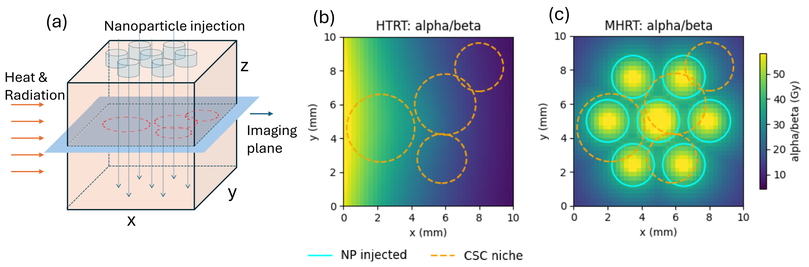

Figure 1. Schematic of the tumor phantom and treatment-specific spatial α/β distribution. (a) Tumor phantom geometry with nanoparticle injection pattern, incident heat/radiation direction, and the imaging plane. (b) α/β map for HTRT. (c) α/β map for MHRT, showing larger and more spatially distributed α/β elevations centered on NP-injected regions. This pattern indicates that MHRT provides more effective intratumoral heat distribution than HTRT and consequently induces a greater increase in α/β.

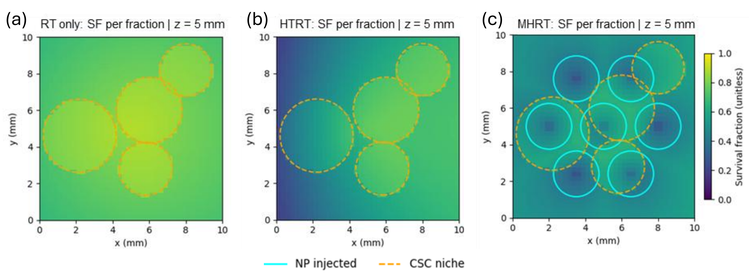

Figure 2. Survival fraction (SF) per fraction maps in the central plane (z = 5 mm) for (a) RT-only, (b) HTRT, and (c) MHRT. CSC niche regions (orange dashed circles) exhibit elevated SF due to radioresistance. Compared with RT-only and HTRT, MHRT shows the most pronounced SF reduction, reflecting the combined effects of nanoparticle-mediated heating and radiation enhancement; cyan solid circles denote NP-injected regions.

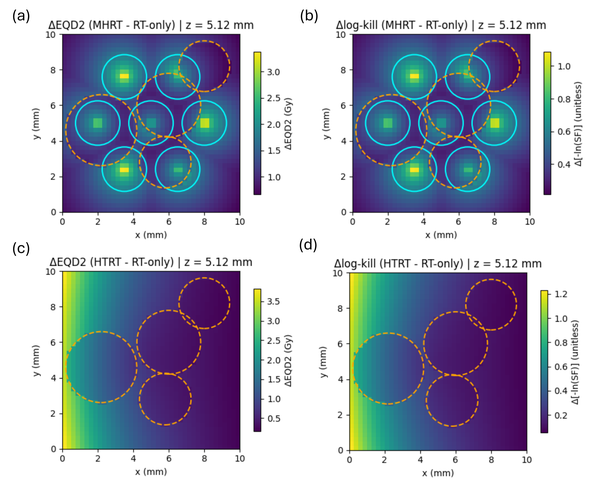

Figure 3. Differential effect maps relative to RT-only in the central plane (z = 5 mm): (a) ΔEQD2 and (b) $\Delta[-\ln(SF)]$ for MHRT, and (c) ΔEQD2 and (d) $\Delta[-\ln(SF)]$ for HTRT. MHRT demonstrates localized biological enhancement near NP-injected regions, whereas HTRT shows a smoother spatial gradient. These spatial patterns correspond to the modality-dependent summary metrics reported in Table 1.

Case	Median −ln(SF_total)	Median EQD2 (Gy)	p50 SF_total	p99 SF_total
RT	0.30	0.94	0.74	0.86
HTRT	0.56	1.75	0.57	0.77
MHRT	0.78	2.42	0.46	0.63

Table 1. Summary of voxel-wise tumor response metrics for RT, HTRT, and MHRT. Median $-\ln(SF_{total})$, median EQD2, and percentile-based SF_{total} values show progressively greater tumor suppression from RT to HTRT to MHRT, with MHRT exhibiting the largest biological effect

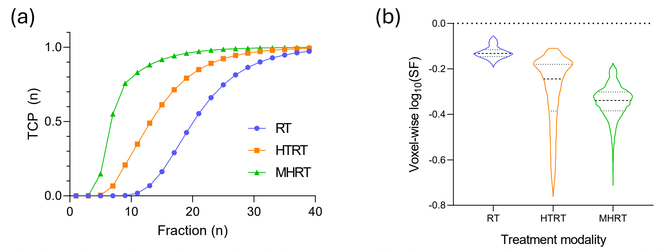

Figure 4. Fractionation-dependent tumor control and voxel-wise survival fraction distribution across treatment modalities. (a) Tumor control probability as a function of fraction number, $TCP(n)$, for RT, HTRT, and MHRT. The curves show systematic modality-dependent separation, with MHRT achieving earlier and steeper tumor control than HTRT and RT. (b) Violin plots of voxel-wise $\log_{10}(SF)$ summarizing survival fraction distributions for each modality. Compared with RT, both HTRT and MHRT shift the distribution toward lower survival, and MHRT exhibits the most pronounced expansion of the low-survival subpopulation, consistent with its superior TCP response.

CONCLUSION

Fractionation-aware voxel-based analysis demonstrated consistent modality-dependent separation, with MHRT producing the strongest biological effect, the deepest low-survival subvolumes, and the earliest rise in TCP compared with HTRT and RT under identical RT conditions. These findings indicate that localized nanoparticle-mediated heating enhances tumor control beyond uniform hyperthermia, and that distribution-level survival heterogeneity, rather than median response alone, is a key driver of treatment gain.

REFERENCES

1. Heo, D, *et al.* Quantitative analysis of radiosensitizing effect for magnetic hyperthermia-radiation combined therapy on prostate cancer cells, *Medical Physics* **50**(10), 7606-7618 (2024)
2. van Leeuwen, C. M. *et al.* Measurement and analysis of the impact of time-interval, temperature and radiation dose on tumour cell survival and its application in thermoradiotherapy plan evaluation. *International Journal of Hyperthermia* **34**(1), 30–38 (2018).
3. van Leeuwen, C. M., Crezee, J., Oei, A. L., Franken, N. A. P., Stalpers, L. J. A., Bel, A., and Kok, H. P. The effect of time interval between radiotherapy and hyperthermia on planned equivalent radiation dose. *International Journal of Hyperthermia* **34**(7), 901-909 (2018).
4. Rajan, A. & Sahu, N. K. Review on magnetic nanoparticle-mediated hyperthermia for cancer therapy. *Journal of Nanoparticle Research* **22**, 1–25 (2020).

ACKNOWLEDGEMENTS

Basic Science Research Program supported this research through the National Research Foundation of Korea (NRF), funded by the Ministry of Education (2021R1A6A3A14044558), and INOBIOGEN Inc. (AURI-37987).

CONTACT INFORMATION
Corresponding Author: Dr. C. Huh
Email: chuh@augusta.edu

GEORGIA CANCER CENTER
AUGUSTA UNIVERSITY